J Biol Inorg Chem (2009) 14:801–811
DOI 10.1007/s00775-009-0493-9

ORIGINAL PAPER

Mechanistic insight into the initiation step of the reaction of *Burkholderia pseudomallei* catalase-peroxidase with peroxyacetic acid

Ben Wiseman · Julie Colin · Andrew T. Smith · Anabella Ivancich · Peter C. Loewen

Received: 10 December 2008 / Accepted: 1 March 2009 / Published online: 17 March 2009

Abstract The reaction of the catalase-peroxidase of *Burkholderia pseudomallei* with peroxyacetic acid has been analyzed using stopped-flow spectrophotometry. Two well-defined species were observed, the first defined by an increase in intensity and narrowing of the Soret band at 407 nm and a 10-nm shift of the charge transfer band from 635 to 625 nm. These features are consistent with a ferric spectrum with a greater proportion of sixth-coordination character and are assigned to an Fe^{III}–peroxyacetic acid complex. Complementary 9-GHz EPR characterization of the changes in the ferric signal of the resting enzyme induced by the binding of acetate in the heme pocket substantiates the proposal. Kinetic analysis of the spectral changes as a function of peroxyacetic acid concentration revealed two independent peroxyacetic acid binding events, one coincident with formation of the Fe^{III}–peroxyacetic acid complex and the other coincident with the heme oxidation to the subsequent ferryl intermediate. A model to explain the need for two peroxyacetic acid binding events is proposed. The reaction of the W330F variant followed similar kinetics, although the characteristic spectral features of the Fe^{IV}=O $Por^{\bullet+}$ species were detected. The variant D141A lacking an aspartate at the entrance to the heme cavity as well as the R108A and D141A/R108A variants showed no evidence for the Fe^{III}–peroxyacetic acid complex, only the formation of ferryl species with absorbance maxima at 414, 545, and 585 nm.

Keywords Catalase-peroxidase · Enzyme–peroxyacetic acid complex · Ferryl heme iron · Compound I · EPR spectroscopy

Electronic supplementary material The online version of this article (doi:10.1007/s00775-009-0493-9) contains supplementary material, which is available to authorized users.

B. Wiseman · P. C. Loewen (✉)
Department of Microbiology,
University of Manitoba,
Winnipeg, MB R3T 2N2, Canada
e-mail: ploewen@ms.umanitoba.ca

J. Colin · A. Ivancich (✉)
Centre d'Etudes de Saclay,
IBITEC, Service de Bioénergétique,
Biologie Structurale et Mécanismes,
CNRS URA 2096, Bat 532,
91191 Gif-sur-Yvette, France
e-mail: anabella.ivancich@cea.fr

A. T. Smith
Department of Chemistry and Biochemistry,
School of Life Sciences, University of Sussex,
Brighton BN1 9QG, UK

Introduction

Catalase-peroxidases (KatGs) found in bacteria, archaebacteria, and some fungi are multifunctional enzymes capable of catalyzing a diverse range of chemical reactions, including catalase, peroxidase, INH lyase, NADH oxidase, and isonicotinoyl-NAD synthase reactions [1, 2]. The enzyme was first purified from *Escherichia coli* in 1979 [3] and genetically mapped in 1985 [4] as being encoded by the *katG* gene, which was then sequenced in 1988 [5], and interest in it increased significantly when its role in the activation of INH as an antitubercular drug was reported in 1992 [6]. Since then numerous studies have focused on defining the detailed reaction pathways involved in the catalase and peroxidase reactions leading to INH activation.

The reaction cycle of both monofunctional catalases and peroxidases starts with the oxidation of the heme to form an

oxyferryl porphyrin cation radical species, Fe^{IV}=O $Por^{\bullet+}$, commonly named "compound I." While H_2O_2 is the natural oxidizing substrate, organic peroxyacids such as peroxyacetic acid (PAA) and *m*-chloroperoxybenzoic acid (mCPBA) can also oxidize the heme to the Fe^{IV}=O $Por^{\bullet+}$ intermediate. Catalases utilize H_2O_2 as a two-electron donor in the second stage to reduce Fe^{IV}=O $Por^{\bullet+}$ back to the resting state, generating molecular oxygen and water. Peroxidases, on the other hand, utilize one-electron donors as substrates in two sequential reduction reactions to return Fe^{IV}=O $Por^{\bullet+}$ to the resting state. In cytochrome *c* peroxidase [7] and lignin peroxidase [8], an alternative intermediate Fe^{IV}=O $Trp^{\bullet}$, formed via intramolecular electron transfer between the tryptophan and the porphyrin, is reduced by either cytochrome *c* or veratryl alcohol, respectively. KatGs have been shown to behave as catalases in the presence of H_2O_2, but they also utilize alternative protein-based intermediates such as cytochrome *c* peroxidase and lignin peroxidase when electron donors are available as substrates [9]. There have been several UV–vis spectrophotometric analyses of the reaction of KatGs, in particular those from *Synechocystis* (SyKatG) and *Mycobacterium tuberculosis* (MtKatG), with various oxidizing agents, including H_2O_2, PAA, mCPBA, and *tert*-butyl hydroperoxide, with the aim of understanding the reaction pathway on a millisecond time scale [10–17]. The most common pattern of spectral changes included a decrease in intensity of the Soret band accompanied by changes in the charge transfer (CT) bands consistent with a rapid one-step reaction leading to the formation of Fe^{IV}=O $Por^{\bullet+}$ and a ferryl-like species [10–16], although a two-step process in which the first species exhibited an increase in intensity of the Soret band and a 10-nm shift of the ferric CT band prior to the appearance of a ferryl-like spectrum has also been reported [17]. This two-step process was explained in terms of a novel reaction pathway beginning with the transient formation of an Fe^{III} $AA^{\bullet}$ species (defined as compound II) and followed by its conversion to an Fe^{IV}=O $Por^{\bullet+}$ $AA^{\bullet}$ species (defined as hypervalent compound I) [17]. More recently, a similar two-step reaction was reported for KatG from *Burkholderia pseudomallei* (BpKatG) upon treatment with PAA [16], but the identity and kinetics of formation were not addressed beyond the observation that a transient intermediate preceded the formation of compound I. The detection of a species distinct from the resting state and the oxoferryl state exhibiting electronic absorption spectral features consistent with a ferric oxidation state of the heme was intriguing and raised a number of questions, including what factors affected its formation, why had it been observed in only one study of MtKatG, and why was it not detected in SyKatG. Interestingly, a seemingly equivalent case was reported for the reaction of ferric cytochrome P450cam enzyme with peroxyacids, in which evidence for an enzyme–peroxyacid complex en route to the formation of compound I was found in stopped-flow spectrophotometric studies [18].

In the current work we focused on the initial step of the reaction of BpKatG with PAA and mCPBA, taking advantage of the slower reaction of this enzyme as compared with SyKatG [16]. Our findings indicate that the properties of the transient species formed within 30 ms after mixing BpKatG with PAA are consistent with it being an Fe^{III}–PAA complex, which precedes the binding of a second molecule of PAA leading to the formation of the high-valent oxoferryl intermediate(s). Complementary 9-GHz EPR characterization of the changes in the ferric signal of the resting enzyme induced by the binding of acetate in the heme pocket substantiates the proposal. A model describing the sites of sequential binding of two PAA molecules and the role of the second PAA in the subsequent oxidation of the heme iron is proposed on the basis of the crystal structure of the enzyme.

Materials and methods

Protein and biochemicals

The wild-type and variant strains of BpKatG were produced, isolated, and purified as previously described [19]. PAA, mCPBA, H_2O_2, and 2,2′-azinobis(3-ethlybenzothiazolinesulfonic acid) (ABTS) (all at the highest available grade) were purchased from Sigma-Aldrich.

Enzyme assays

Catalase activity was determined by the method of Rørth and Jensen [20] in a Gilson oxygraph equipped with a Clark electrode. One unit of catalase is defined as the amount that decomposes 1 μmol of H_2O_2 in 1 min in a 60 mM H_2O_2 solution at pH 7.0 and 37 °C. Peroxidase activity was determined spectrophotometrically using ABTS [21] as an electron donor. One unit of peroxidase activity is defined as the amount that decomposes 1 μmol of ABTS in 1 min in a solution of 1 mM ABTS (ε_{405} = 36,800 M^{-1} cm^{-1}) and 1.25 mM H_2O_2 in 50 mM sodium acetate buffer, pH 4.5 at 25 °C. The enzyme was appropriately diluted and 20–100 nmoles of enzyme monomer was assayed. Enzyme assays involving manual mixing were carried out using Pharmacia Ultrospec 4000 or Biochrom Ultrospec 3100 Pro spectrophotometers. The protein was estimated according to the method of Layne [22]. Manually mixed absorption spectra were recorded using a Milton Roy MR300 spectrophotometer. In all cases experiments were performed at 25 °C in 1-mL quartz

semimicro cuvettes. Unless otherwise stated, protein was diluted in 50 mM potassium phosphate buffer, pH 7.0 and the same buffer was used as a reference.

Stopped-flow UV–vis absorption measurements

The time-dependent absorption spectra were obtained using a four-syringe SX20 stopped-flow spectrophotometer (Applied PhotoPhysics) equipped for conventional and sequential stopped-flow measurements with an attached diode-array detector. A refrigerating bath (Huber Minichiller) was used to regulate the temperature of the samples in the syringes and in the mixing cell to 25 °C. All measurements were performed using an optical cell with a path length of 1 cm, and the shortest time for mixing and recording the first data point was 1.26 ms. The enzyme samples were at an initial concentration of 8 μM and were mixed with an equal volume of PAA at the desired excess (see "Results"). The buffers used for the measurements at pH 4.5, 7.0, and 8.5 were sodium acetate, potassium phosphate, and tris(hydroxymethyl)aminomethane (Tris)–HCl, respectively, all at 50 mM concentration, both for the enzyme and for the PAA and mCPBA solutions. Buffer exchange was done using Centricon Y10 microconcentrators (Amicon). Data were recorded using 500 data points on a logarithmic scale and over a total time of 20 s. Data analysis was done using singular-value decomposition with the Pro-K.2000 Global Analysis program (Applied PhotoPhysics) to fit the time-dependent spectra and obtain the observed transition rate constants ($k_{1,2,\ldots,n}$) between species. Single-wavelength measurements were performed at 409 nm with 4 μM protein and increasing amounts of peroxyacids to determine the concentration dependency of the enzyme reaction with PAA and mCPBA. Reaction rate constants (k_A and k_B) were determined simultaneously by fitting the time traces obtained at 409 nm to a double-exponential equation for the various PAA and mCPBA concentrations using the curve-fitting application in the Pro-Data Viewer software (Applied PhotoPhysics).

EPR spectroscopy measurements

Low-temperature (4 K) 9-GHz EPR measurements were performed using a Bruker ER 300 spectrometer with a standard TE_{102} cavity equipped with a liquid helium cryostat (Oxford Instruments) and a microwave frequency counter (Hewlett-Packard 5350B). EPR samples were measured as frozen solutions in 4-mm quartz tubes. To avoid the previously described effect of pH drop of the phosphate buffer when freezing the samples, 50 mM Tris–maleate buffer was used for the EPR measurements [9]. The choice of pH 6.4 was made on the basis of the similar ratio of both signals contributing to the resting enzyme's EPR signal [23]. Samples were prepared by buffer exchange using Centricon Y10 microconcentrators (Amicon) and 50 mM Tris–maleate buffer at pH 6.4. For the acetate effect tests, a 30-μL enzyme sample (initial concentration 0.5 mM) at pH 6.4 was mixed with 10 μL sodium acetate buffer (initial concentration 200 mM) at pH 5.8; the final pH of the sample was determined to be 6.24.

Model building of PAA binding

The models showing PAA bound in the heme cavity of BpKatG were constructed manually using the program Coot [24] starting with coordinates taken from the native crystal structure (PDB accession code 1MWV). When PAA interactions with the protein were tested, rotation was allowed only around the O–O bond of PAA, and the protein structure was maintained rigid. Only hydrogen bonds with favorable geometry were allowed and unfavorable steric interactions differing from optimal van der Waals interactions were not allowed. The oxygens of PAA were placed in close proximity to the locations of displaced waters to maintain as much of the matrix feature as possible, because disruption of the water matrix (Fig. 6a) affects enzymatic activity [23, 25] and the matrix water molecules have B factors similar to those of the adjacent protein atoms, suggesting a close association. Only two waters (3085 and 2653 in 1MWV) were removed and one water (3897 or W1) was shifted 0.5 Å to accommodate PAA1.

Results

Reaction of wild-type BpKatG with PAA

Figure 1 shows the changes of the electronic absorption spectrum of BpKatG at pH 7.0 upon reaction with 50-fold excess of PAA and as a function of time on a millisecond time scale up to 20 s. The resting enzyme shows the Soret band at 407 nm and a CT band at 635 nm, characteristic of the ferric oxidation state (Fig. 1, black trace). After the enzyme had been mixed with PAA, a 10% intensity increase and narrowing of the Soret band with a concomitant shift of the CT band to 625 nm (Fig. 1, gray arrows) are observed within 30 ms (Fig. 1, thick gray trace). A new spectrum is observed after 400 ms (Fig. 1, red trace), with the main features being a shift in the Soret band to 414 nm (and an evident shoulder at about 420 nm) and a concomitant appearance of two bands at 545 and 585 nm. Additional features of this complex spectrum are the decrease in intensity of the Soret band and the appearance of a broad ill-defined shoulder at around 655 nm. Spectral analysis of the rapid-scan electronic absorption spectrum of the reaction of BpKatG with a 50-fold excess of PAA showed a good fit to the experimental data when using a

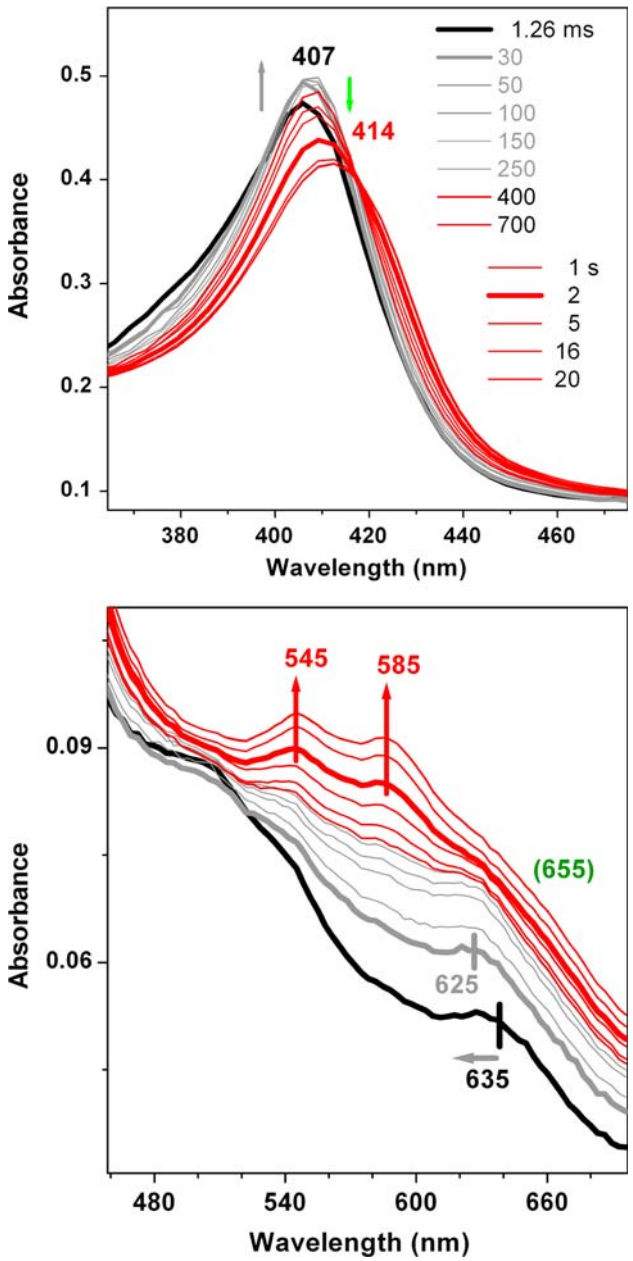

Fig. 1 Rapid-scan electronic absorption spectra of the reaction of wild-type *Burkholderia pseudomallei* catalase-peroxidase (BpKatG) at pH 7.0 with 50-fold excess of peroxyacetic acid (PAA). Selected spectra representing the resting (ferric) enzyme (*black trace*), the Fe^{III}–PAA complex (*thick gray trace*), and the transition to the ferryl-like intermediate (*red traces*) are shown. The experimental conditions were 25 °C reaction temperature, 4 μM enzyme, and 200 μM PAA (final) concentrations. Data were recorded on a logarithmic time scale over a total period of 20 s

model of three species and two rates (A → B → C, transition rates of $k_1 = 17\ s^{-1}$ and $k_2 = 1\ s^{-1}$), with species A being the ferric enzyme (Fig. 1, black trace). The spectrum of species B (Fig. 1, thick gray trace) differs from that of the resting (ferric) state in the clear increase in intensity of the Soret band and the 10-nm upshift of the CT band. This is an indication of the heme iron still being in the ferric oxidation state, yet with subtle changes in the iron coordination. Very similar changes in the electronic absorption spectrum of horseradish peroxidase were observed when benzohydroxamic acid was bound to the distal heme side [26], the latter being assigned to a greater proportion of six-coordination induced by the binding of benzohydroxamic acid [27]. Similarly, the spectral changes of species B in BpKatG are consistent with a conversion from a mixture of five- and six-coordinated high-spin heme to a more six-coordinated case, as a result of a small but significant perturbation of the hydrogen-bonding network on the heme distal side.

We have previously demonstrated that the EPR spectrum of the resting BpKatG enzyme can be used to monitor subtle changes in the hydrogen-bonding network from the heme distal side induced by pH [23] and/or mutations of distal side residues [25]. Accordingly, we used acetate as a model for the putative effect of binding of PAA to the heme distal side as monitored by the changes in the ferric EPR spectrum and the corresponding changes in the UV–vis electronic absorption spectrum. Figure 2 shows the effect of adding 130-fold excess of acetate buffer at pH 5.8 (top spectrum, red trace) to the ferric wild-type enzyme at pH 6.4 (top spectrum, black trace). A change in the relative contribution to the EPR spectrum of the rhombically distorted ($g_{Bx} = 6.50$, $g_{By} = 5.10$, and $g_{Bz} = 1.97$) and axial ($g_{A\perp} = 5.90$ and $g_{A\parallel} = 1.99$) signals was observed upon addition of acetate buffer to the enzyme. A pH effect can be ruled out because the final pH of the sample was 6.24 and, as we have previously demonstrated, there is no change in the ferric EPR signal for the range $5.6 \leq pH \leq 6.6$ [23]. The electronic absorption spectra of the sample used for the EPR experiments showed an evident increase in intensity and narrowing of the Soret band with a concomitant 10-nm upshift of the CT band upon addition of 130-fold acetate (Fig. 2, insets, red trace). In fact, these changes of the electronic absorption spectrum of BpKatG upon addition of acetate were the same as those observed within 30-ms mixing time in the reaction with PAA (Fig. 1, thick gray trace). Similarly, a change in rhombicity of the EPR spectrum was observed in horseradish peroxidase upon binding of benzohydroxamic acid, with the corresponding same changes in the UV–vis electronic absorption spectrum [26]. A similar effect on the rhombicity of the ferric EPR signal was previously reported upon binding of formate in the heme distal side of a monofunctional catalase and was confirmed by the crystal structure of the formate-bound enzyme [28]. Therefore, given that specific binding in the heme cavity can cause subtle changes both in the absorption and in the EPR spectra of catalases and peroxidases, we conclude

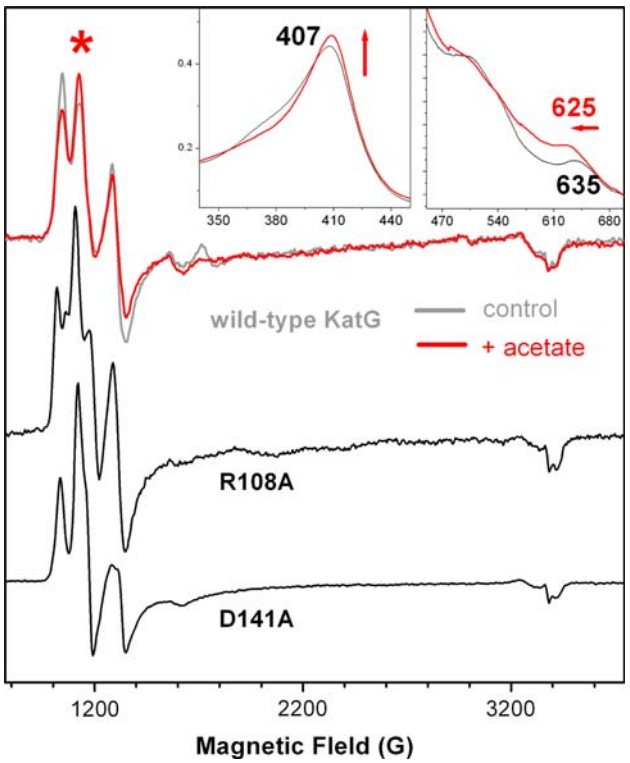

Fig. 2 9-GHz EPR spectra of the resting (ferric) BpKatG at initial pH 6.5 (*top*, *gray trace*) upon incubation with 130-fold excess of sodium acetate at pH 5.8 (*top*, *red trace*). The *red asterisk* indicates the higher contribution of the axial component ($g_{A\perp} = 5.90$ and $g_{A\parallel} = 1.99$) of the ferric EPR spectrum induced by acetate binding. The *inset* shows the electronic absorption spectra of the same EPR samples. The spectral changes induced by incubation in acetate are the same as those of the Fe^{III}–PAA complex (Fig. 1, thick gray trace). The EPR spectra of the R108A (*middle*) and D141A (*bottom*) variants at pH 6.5, also having higher contribution of the axial signal induced in both cases by the mutations [23], are shown for comparison. The experimental conditions were 4 K, 4-G modulation amplitude, 1-mW microwave power, and 100-kHz modulation frequency. The final pH of the enzyme incubated in acetate was 6.24

that species B in the reaction of BpKatG with PAA is a complex between the enzyme and one molecule of PAA, to be called the Fe^{III}–PAA complex.

The predominant features of the electronic absorption spectrum of species C (Fig. 1, solid red trace) agree well with those expected for a ferryl species in heme peroxidases, exhibiting a shift of the Soret band to 414 nm and two CT bands at 545 and 585 nm. As mentioned before, other features contribute to the spectrum (see below), possibly reflecting the limitations of the singular-value decomposition analysis in defining the spectrum of intermediates with unambiguous physical significance in this case. The wavelengths defining the bands of the ferryl species remain unchanged for several minutes, until a slow transition to the resting state ferric spectrum is observed. Simultaneous monitoring of the absorbance of the O–O bond of PAA revealed its slow disappearance (Fig. S1), suggesting that the return to the resting state is associated with depletion of the PAA. Therefore, the changes in the relative intensities of the band of the ferryl species occurring after 400 ms in the wild-type BpKatG electronic absorption spectrum (Fig. 1, red traces) represent subtle changes in the steady state of intermediates involved in the metabolism of PAA as its concentration is depleted. The reaction pathway for PAA depletion remains a matter of conjecture.

The additional features in the ferryl spectrum are indicative of the contribution of an Fe^{IV}=O $Por^{\bullet+}$ species, called compound I in horseradish peroxidase (for a review see [29]). The contribution of these two species to the spectrum is better illustrated by the pH dependence of the reaction (Fig. 3a); the ferryl-like spectrum is predominant at pH 4.5 (Fig. 3a, red trace), while the characteristic features of the Fe^{IV}=O $Por^{\bullet+}$ species are better defined at pH 8.5 (Fig. 3a, dark green trace). Moreover, the W330F variant, in which the proximal-side Trp has been replaced by Phe, showed a spectrum with a clearly more pronounced decrease in intensity (50%) of the Soret band and a concomitant better resolved broad band at 655 nm, as compared with the wild-type case (Fig. 3b), indicating a longer-lived Fe^{IV}=O $Por^{\bullet+}$ species. It is noteworthy that while the electronic absorption spectrum shows well-characterized features for the Fe^{IV}=O $Por^{\bullet+}$ species because delocalization of the radical over the porphyrin molecule directly affects its electronic structure [29], it is certainly not possible to distinguish an Fe^{IV}=O species (compound II in horseradish peroxidase) from an Fe^{IV}=O $Trp^{\bullet}$ or an Fe^{IV}=O $Tyr^{\bullet}$ species solely on the basis of the electronic absorption spectrum, as we have previously demonstrated using EPR spectroscopy combined with stopped-flow spectrophotometry [30]. The detailed characterization of the ferryl-like intermediate(s) in BpKatG requires multifrequency EPR spectroscopy combined with isotope labeling and site-directed mutagenesis (see, e.g., [9, 31]), putting it beyond the scope of this work, and it will be reported separately.

Evidence for two separate PAA binding events

To determine the order of reaction for the formation of the two species B and C, the concentration of PAA was increased over the range 50–500 μM. The reaction rates k_A and k_B for the transitions A → B and B → C, respectively, were determined by monitoring the absorbance at 409 nm as a function of PAA concentration (Fig. 4a) and fitting the change in absorbance to a double-exponential equation. The fast initial step ($k_A = 6.47 \pm 0.45 \times 10^4\ M^{-1}\ s^{-1}$) represented by the increase in intensity of the Soret band followed by the subsequent slower redshift and decrease in intensity ($k_B = 2.50 \pm 0.20 \times 10^3\ M^{-1}\ s^{-1}$) are clearly

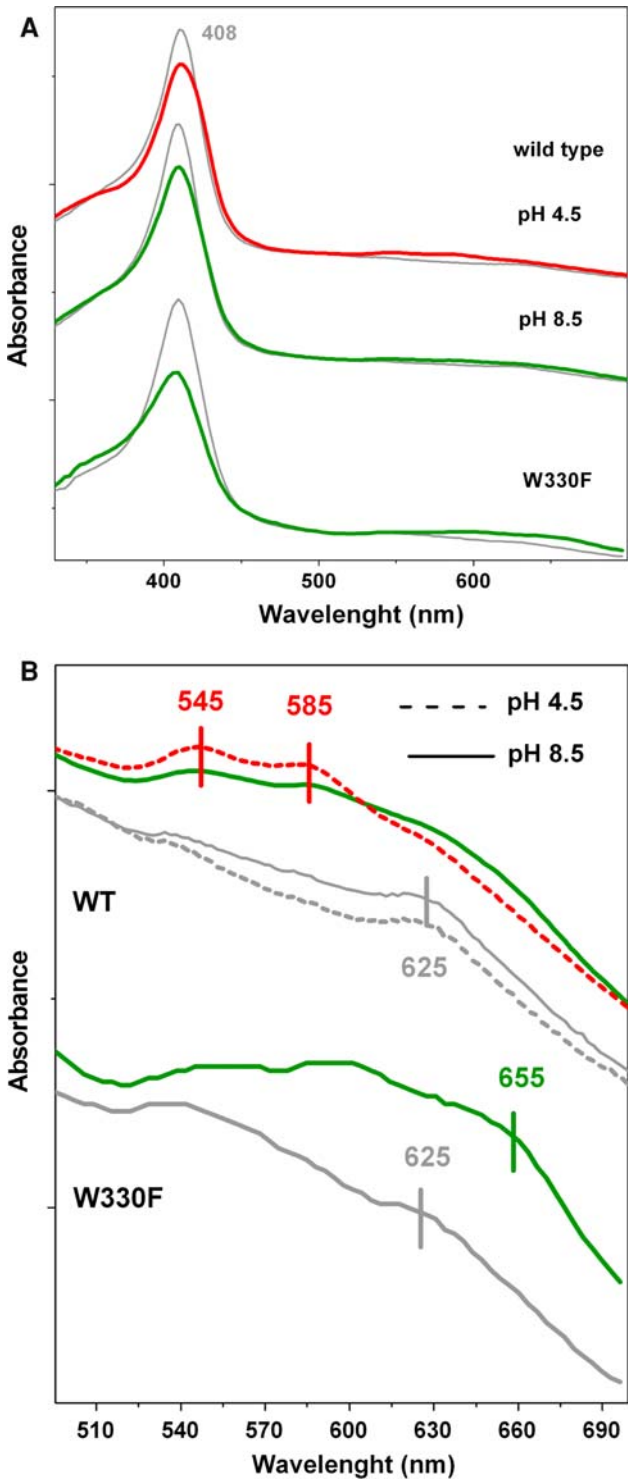

◀ **Fig. 3** **a** Comparison of the rapid-scan electronic absorption spectra obtained in the reaction of wild-type BpKatG at pH 8.5 and 4.5 with 100-fold excess PAA and of the W330F variant at pH 7.0 with 50-fold excess PAA. Only the spectra representative of the Fe^{III}–PAA complex (*gray traces*, 200 ms) and the subsequent intermediate (*red trace* for wild-type BpKatG at pH 4.5 and *dark green trace* for wild-type BpKatG at pH 8.5, both at 5 s) are shown for clarity, and correspond to species B and C in the fitted spectra shown in Fig. 1. **b** The 500–700-nm range of the spectra and the curves corresponding to the wild type at the two pH values are superposed. The decrease in intensity of the Soret band and the broad charge transfer band at 650 nm, characteristic of the Fe^{IV}=O $Por^{\bullet+}$ species, are the predominant features for the W330F variant and the wild-type enzyme at pH 8.5. The experimental conditions were as for Fig. 1

evident. Both rates show a linear dependence on PAA concentration as shown in Fig. 4b, the value of k_B being 3.8% of that of k_A (Fig. 4b, inset). That is to say, the data are consistent with two separate PAA-related events or two second-order steps, the first leading to the formation of the Fe^{III}–PAA complex (species B) and the second leading to the formation of the ferryl species (species C) via the reaction of the Fe^{III}–PAA complex with a second molecule of PAA. The same pattern of spectral changes and order of reaction were observed with mCPBA, consistent with a three-species, two-rate model, but with reaction rates that were 10 times faster ($k_A = 4.43 \pm 0.16 \times 10^5$ M^{-1} s^{-1} and $k_B = 3.10 \pm 0.07 \times 10^4$ M^{-1} s^{-1}) compared with those obtained with PAA.

Influence of specific mutations on the reaction pathway

Mutation of Trp330 in BpKatG elicited a number of subtle changes that are evident in the kinetic parameters of the W330F variant as compared with the wild-type enzyme, including slightly reduced catalase- and peroxidase-specific activities but a faster peroxidase turnover rate. The rapid-scan spectra for the reaction of the W330F variant with a 50-fold excess of PAA resulted in the formation of the same initial Fe^{III}–PAA complex (Fig. 3b, gray trace), but at a rate that was too rapid for k_A to be accurately determined. The rate of the second transition, B → C, was similar to that of the native enzyme ($k_B = 2.60 \pm 0.10 \times 10^3$ M^{-1} s^{-1} with PAA and $1.10 \pm 0.07 \times 10^4$ M^{-1} s^{-1} with mCPBA). As mentioned before, the predominant CT band at 650 nm of the subsequent intermediate (species C) together with the marked decrease in intensity of the Soret band is indicative of a higher contribution of the Fe^{IV}=O $Por^{\bullet+}$ (Fig. 3a, green trace) to the ferryl-like species. A similar situation was observed in the W191F variant of cytochrome *c* peroxidase, where the rapid-scan spectra of the reaction with H_2O_2 suggested the contribution of the Fe^{IV}=O $Por^{\bullet+}$ (as detected by the decrease in intensity of the Soret band) to the ferryl-like spectrum [32].

Residue Asp141 is located in the entrance channel to the heme and along with Arg108 is part of the crucial hydrogen-bonding network on the heme distal side. Mutation of both residues individually significantly reduced catalase activity, but had a lesser effect on peroxidase activity [25], and the EPR spectra of the resting state in both variants were consistent with changes in the extended hydrogen-

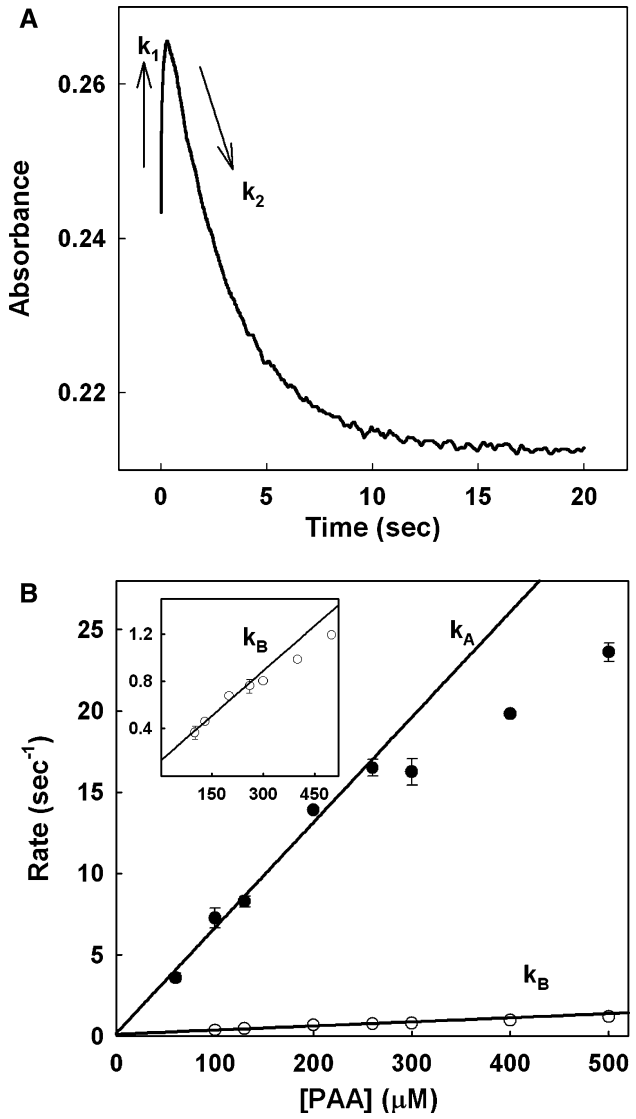

Fig. 4 **a** Time course of the change in absorbance at 409 nm for the reaction of wild-type BpKatG with a 50-fold excess of PAA. The transition rates k_1 and k_2 were determined for the transitions A → B and B → C. **b** PAA dependence of the transition rates k_1 and k_2. The transition rates were determined at different concentrations of PAA and the *inset* shows the plot of k_2 values with a smaller scale to illustrate the dependence on PAA. These data were fitted to a double-exponential equation to determine the bimolecular rate constants k_A and k_B

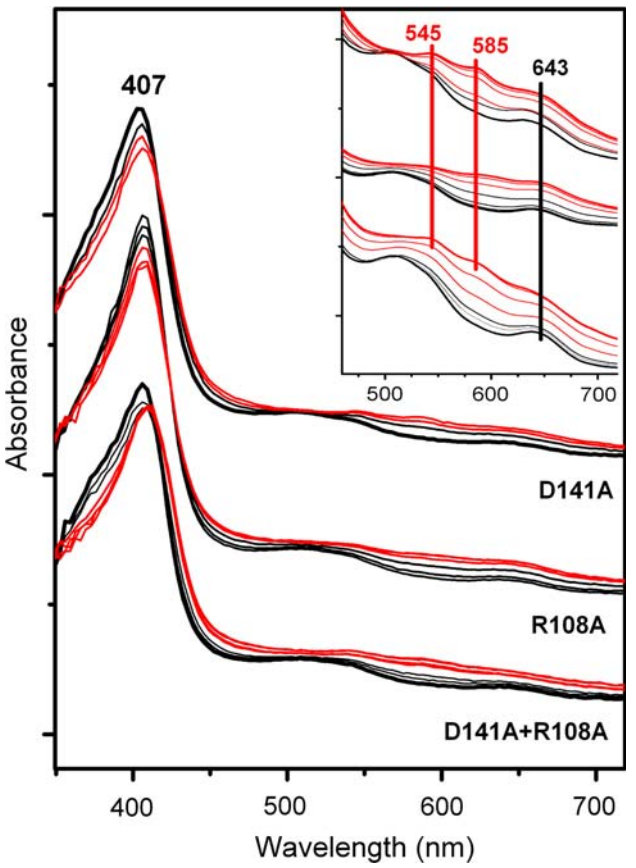

Fig. 5 Rapid-scan electronic absorption spectrum of the reaction of BpKatG variants (D141A, R108A, and D141A/R108A) at pH 7.0 with a 50-fold excess of PAA. Selected spectra representing the resting (ferric) enzyme (*black traces*) and the transition to the ferryl-like intermediate (*red traces*) are shown. The spectra correspond to mixing times of 1.26 ms, 78 ms, 400 ms, 1.7 s, 3 s, 5 s, and 10 s. At variance with the wild-type enzyme, no Fe^{III}–PAA complex (Fig. 1, gray trace) is detected and the ferryl-like species (*red trace*) is detected within 78 ms for D141A, 1.7 s for D141A/R108A, and 3 s for R108A. The experimental conditions were as for Fig. 1. The *inset* shows the 470–725-nm range of the spectra obtained when using more concentrated enzyme (100 μM) and a 15-fold excess of PAA, to better resolve the bands in this region. These spectra correspond to mixing times of 1.26 ms, 10 ms, 50 ms, 500 ms, 2 s, 5 s, and 10 s. At variance with the wild-type enzyme and the W330F variant (Fig. 3b), the charge transfer band of the resting (ferric) enzymes at 643 nm persists during the reaction

bonding network [23]. Therefore, anticipating that both residues might affect the formation of the Fe^{III}–PAA complex, we obtained the rapid-scan spectra of the reaction of the D141A, R108A, and D141A/R108A variants with a 50-fold excess of PAA at pH 7. In contrast to the wild-type and W330F cases, no spectral changes consistent with the formation of the Fe^{III}–PAA complex could be detected in the three variants (Fig. 5). Another clear difference was the contribution of the resting enzyme suggested by the persistence of the CT band at 643 nm throughout the reaction in all three variants (Fig. 5, inset). However, all three variants did resemble the wild-type enzyme in presenting spectral changes consistent with the formation of ferryl-like species. Interestingly, the CT bands at 545 and 585 nm of the ferryl-like species are observed within 80 ms in the case of D141A (Fig. 5, red trace), indicating that the reaction with PAA proceeded much faster than for the wild-type enzyme. The spectral analysis of the time-dependent experimental data using a one-step model

(A → C, where C shows the same spectral features as species C of the wild-type enzyme in Fig. 1) reproduced well the observed spectral changes of the D141A variant, with the rate for A → C being 15 s^{-1} as compared with 1 s^{-1} for the wild-type enzyme. In the case of the D141A/R108A and R108A variants, the reaction is clearly slower than for D141A. The features of the ferryl species (Fig. 5, thick red traces) are only detected after 1.7-s reaction time and the transition rates, 0.9 s^{-1} for D141A/R108A and 0.4 s^{-1} for R108A, obtained from the spectral analysis using a one-step model (A → C, or ferric to ferryl-like species) were comparable to those for the equivalent B → C transition in the wild-type enzyme. In conclusion, a Fe^{III}–PAA complex does not seem to form in any of the single or double Arg108 and Asp141 variants, possibly as a result of the absence of residues involved in ligand binding and of changes in the heme distal side reflected by their ferric EPR spectra (Fig. 2). The possibility that the Fe^{III}–PAA complex forms within the dead-time of the stopped-flow instrument cannot be ruled out, but the proposed rationale remains valid.

Discussion

We have focused on the characterization by stopped-flow spectrophotometry of the initial steps of the reaction of BpKatG with PAA using the advantageous slower reaction of this enzyme as compared with other KatGs [16]. There have been several reports of the rapid-scan reaction of KatGs with PAA and at least two of them have reported a sequence of spectral changes similar to those reported here. Although the species that we have assigned to the Fe^{III}–PAA complex was not observed in the spectrum shown by Jakopitsch et al. [16], the short-lived increase in intensity of the Soret band is clearly evident in the trace of absorbance at 407 nm monitored as a function of time. The latter was described as a hypochromic change in the text and was attributed to a transient intermediate in the reaction pathway, with no speculation as to its identity [16]. The spectra of the reaction of MtKatG with PAA presented in the same study [16] did not exhibit an increase in the Soret band, presenting only the appearance of a ferryl-like spectrum, and a similar outcome was reported for the oxidation of MtKatG by mCPBA by Chouchane et al. [10]. By contrast, a clear two-step reaction pathway for the oxidation of MtKatG by PAA was reported by Ghiladi et al. [17] and, while the pattern of spectral changes was very similar to what we observed in this work for BpKatG, a very different assignment of intermediate identities was presented. The initial species (increase in the Soret band intensity and upshift of the CT band) was assigned to a compound II intermediate despite the differences from the typical compound II spectrum of monofunctional peroxidases. A possible explanation given for the unusual features of the proposed compound II intermediate was the π-stacking interaction of the Trp portion of the Trp-Tyr-Met adduct 3.4 Å above the heme plane causing an alteration in the electronic transitions responsible for the spectrum. The alternative explanation given by Ghiladi et al. implied that MtKatG undergoes an unusual one-electron oxidation to form an Fe^{IV}=O AA species that rapidly and stoichiometrically equilibrated to an Fe^{III}–OH $AA^{\bullet}$ species. Such a species could explain the modified ferric spectrum, but there is no evidence of an oxoferryl species in the early spectra and stoichiometric equilibration to 100% Fe^{III}–OH $AA^{\bullet}$ would be a highly unusual occurrence (for a review see [28]). Similarly, the alternative direct oxidation of the protein prior to heme oxidation, producing an Fe^{III} $AA^{\bullet}$ species would imply a reaction so far unprecedented in heme peroxidases.

The interpretation proposed in this work is more straightforward in concept. The initial step involves the formation of an enzyme–substrate complex, Fe^{III}–PAA, and this is followed by the actual oxidation reaction to form a ferryl-like species that includes, as one component, Fe^{IV}=O $Por^{\bullet+}$, the classic compound I. The proposal that the initial species formed upon mixing BpKatG and PAA is an Fe^{III}–PAA complex deserves particularly serious consideration because it presents definite advantages over the previous unusual options [17]. First, the modified ferric spectrum is consistent with that ascribed to a higher proportion in sixth-coordination character of the ferric iron in peroxidases which would be expected during formation of an Fe^{III}–PAA complex [26, 27]. Second, such an enzyme–substrate complex is an expected intermediate in all enzymatic reaction pathways. Third, the subsequent oxidation reaction leads to the expected higher-valence species, including the Fe^{IV}=O $Por^{\bullet+}$ intermediate. Fourth, a simple Fe^{III}–PAA complex does not require the proposal of unusual reactions and intermediates. Fifth, a very similar Fe^{III}–H_2O_2 complex has been identified in the R38L variant of horseradish peroxidase, providing a precedent for such an intermediate [33]. Finally, the reaction of ferric cytochrome P450cam enzyme with PAA followed by stopped-flow spectrophotometry also showed evidence for an acylperoxo complex en route to the formation of compound I [18]. In summary, the arguments in support of assigning the modified ferric spectrum to an Fe^{III}–PAA complex are compelling.

The conclusion that formation of an enzyme–substrate complex precedes the reaction leading to the ferryl species is consistent with long-standing enzyme kinetic theory and is consistent with a model proposed for H_2O_2 binding to monofunctional peroxidases [34]. However, it is novel in so far as such an explanation has not been proposed previously for similar published data describing the oxidation

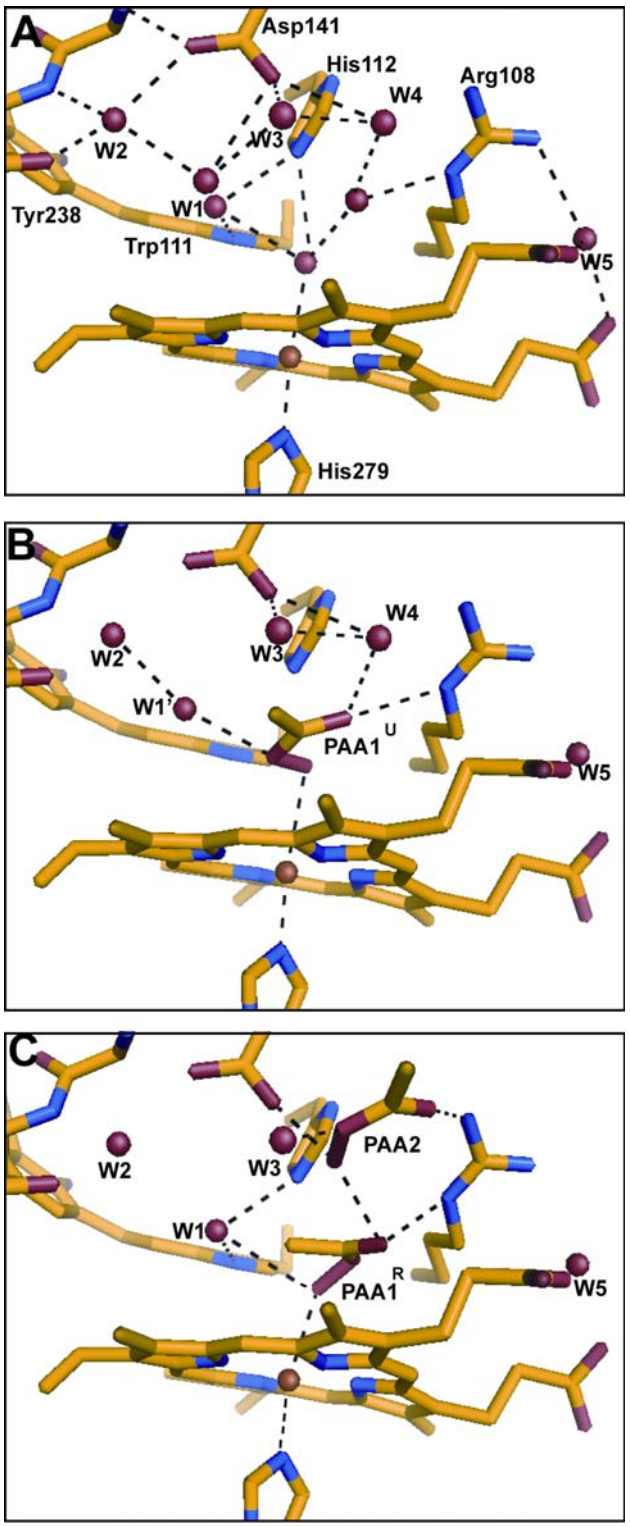

◀ **Fig. 6** Possible binding sites for PAA. In **a**, the heme cavity is shown with no PAA bound to illustrate the water matrix that exists in the resting enzyme. Hydrogen bonds are denoted by the *dashed lines*. In **b**, a putative site for the binding of the first PAA is shown. In **c**, two PAA molecules are shown to illustrate a possible role of the second PAA. The key differences lie in the change in orientation of PAA1 between the structures shown in **b** and **c**. $PAA1^{U}$, the unreactive conformation, is shown in **b** and $PAA1^{R}$, the reactive conformation, is shown in **c** stabilized by the interactions with PAA2. Water W1 moves in the presence of $PAA1^{U}$ to the W1′ location in **b** and back to W1 in **c** in the presence of $PAA1^{R}$. In **b** and **c** only those hydrogen bonds directly influenced by the PAA binding are shown. Waters W2, W3, W4, and W5 are shown in **a**–**c** in their original locations. PAA is shown bound in **a**–**c**, but *m*-chloroperoxybenzoic acid can bind in exactly the same locations, forming the same interactions with minimal interaction with other parts of the protein. The view in all cases is from slightly below the plane of the heme on the proximal side

pathway of KatGs. On the other hand, the conclusion that there are two separate PAA (or mCPBA) binding events leading to heme oxidation is new and provides interesting insights into the reaction. The role of the first PAA binding event, to form the Fe^{III}–PAA or enzyme–substrate complex, is clear. The role of the second PAA binding event is not as obvious, but the fact that it occurs coincidentally as the heme is oxidized to the ferryl intermediate provides a hint as to its role. Arguably the simplest explanation is that the initial Fe^{III}–PAA complex has PAA1 bound in an orientation that is not conducive to heme oxidation, and the second binding event facilitates the reorientation of PAA1 to allow oxidation. Another way of stating this is that there are two binding orientations for PAA1 in proximity to the heme that are in equilibrium, $PAA1^{U} \rightleftharpoons PAA1^{R}$ (where U and R denote unreactive and reactive conformations, respectively). The equilibrium favors $PAA1^{U}$ in the absence of PAA2 and favors $PAA1^{R}$ when PAA2 is bound. One prediction of this model is that at a low concentration of PAA, the binding of PAA2 and the appearance of ferryl intermediates should be much reduced. That is to say, the second transition (B → C) should be less obvious in the spectra, and this was observed experimentally, with ferryl intermediates being only weakly evident in the spectra, despite sufficient reaction to deplete the PAA and return the enzyme to the resting state. Other variations on this concept involving an equilibrium between two binding conformations might also be envisioned.

The heme cavity provides sufficient room to accommodate two PAA molecules (Fig. 6) and even two mCPBA molecules with the planar chlorophenyl rings positioned in the entrance channel (not shown). The extended hydrogen-bonding network in the heme cavity is shown in Fig. 6a, and fitting PAA1 into the cavity displaces two waters molecules and shifts W1 to W1′ (Fig. 6b). The two proposed orientations of PAA1 are shown in Fig. 6b and c, with the second PAA2 bound only in Fig. 6c. That is, a single $PAA1^{U}$ binds with its carbonyl oxygen replacing one of the original matrix waters and forming hydrogen bonds (2.97 Å) with the N–H of the guanidinium of Arg108 and matrix water W4. Additionally, the OH oxygen of PAA^{U} is situated 2.86 Å from the iron and 2.78 Å from the

imidazole N^{ε} of His112 (although the geometry is poor for a hydrogen bond), and 3.22 Å from the indole nitrogen of Trp111 (also with poor geometry for hydrogen bonding). Oxygen O_2 of $PAA1^U$ can form a hydrogen bond with water W1′, which is shifted about 0.5 Å from the original position of W1. The direct involvement of R108 and indirect involvement of Asp141, through water W4, in this binding site is consistent with the apparent absence of Fe^{III}–PAA in the R108A, D141A, and R108A/D141A variants. Orientation $PAA1^R$ (Fig. 6c) would appear to be less stable, with the single hydrogen bond between the noncarbonyl oxygen and Arg108 having poor geometry. Thus, the proposed role for PAA2 is to stabilize the $PAA1^R$ orientation by forming a hydrogen bond with the carbonyl oxygen of PAA1 (2.70 Å). The binding of PAA2 is further stabilized by a hydrogen bond of its carbonyl oxygen with the guanidinium group of Arg108 (2.87 Å), and by hydrogen bonds of the OOH portion with a matrix water and the carbonyl oxygen of Asp141 (2.88 Å).

In addition to the reorientation of the −OOH portion of PAA1, the location of water W1–W1′ in the two orientations determines why $PAA1^R$ is reactive whereas $PAA1^U$ is not. $PAA1^U$ displaces W1 about 0.5 Å to position W1′, where it cannot interact with either His112 or the OOH of PAA1, whereas $PAA1^R$ allows W1 back into the matrix position, sharing hydrogen bonds with the OOH of PAA1 and the N^{ε} of His112. In this position, it can fulfill the same role as the proposed proton transfer water in horseradish peroxidase where the energy barrier for proton transfer is significantly reduced by having a proton shuttled from OOH to the His by a water [35].

The metabolism of PAA by KatGs has been known for some time, but the mechanism underlying the phenomenon remains undefined. One obvious possibility is that the normal complement of Met and Try residues may provide a reservoir of oxidizable residues that can provide electrons for PAA reduction. However, screening for oxidized residues after PAA treatment revealed only a small number of oxidized centers and none of them were stoichiometrically oxidized (Wiseman and Loewen, unpublished data). This leads to the conclusion that PAA undergoes a disproportionation or dismutation reaction in which it serves as both an oxidant and a reductant. Confirmation for such a reaction is so far lacking.

In conclusion, we have shown that PAA oxidation of BpKatG includes the initial rapid formation of an enzyme–substrate complex, within 30 ms, followed by the subsequent formation of a higher-valence intermediate (ferryl species) 400 ms later. Each of the two steps in the reaction pathway is PAA-dependent, implying the need for two PAA molecules for the oxidation, possibly to stabilize binding in a reactive conformation. The need for two PAA molecules also implies the existence of two different binding sites for PAA (or mCPBA) within the tightly constrained access channel and heme pocket. Indeed, the fact that the enzyme–substrate complex formation step is slow enough to be monitored by absorption spectrophotometry in KatGs, unlike monofunctional peroxidases, is most probably related to these steric constraints and the more defined water matrix on the distal side of the heme in KatGs (Fig. 6a).

Acknowledgments This work was supported by the French CNRS and CEA Saclay (to A.I.), a Ph.D. Fellowship (CFR contract from CEA Saclay to J.C.), and grants from the Natural Sciences and Engineering Research Council of Canada (to P.C.L.) and the Canadian Research Chair Program (to P.C.L.).

References

1. Singh R, Wiseman B, Deemagarn T, Donald LJ, Duckworth HW, Carpena X, Fita I, Loewen PC (2004) J Biol Chem 279:43098–43106
2. Singh R, Wiseman B, Deemagarn T, Jha V, Switala J, Loewen PC (2008) Arch Biochem Biophys 417:207–214
3. Claiborne A, Fridovich I (1979) J Biol Chem 254:4245–4252
4. Loewen PC, Triggs BL, George CS, Hrabarchuk BE (1985) J Bacteriol 162:661–667
5. Triggs-Raine BL, Doble BL, Mulvey MR, Sorby PA, Loewen PC (1988) J Bacteriol 170:4415–4419
6. Zhang Y, Heym B, Allen B, Young D, Cole S (1992) Nature 358:591–593
7. Sivaraja M, Goodin DB, Smith M, Hoffman B (1989) Science 245:738–740
8. Blodig W, Smith AT, Winterhalter K, Piontek K (1999) Arch Biochem Biophys 370:86–92
9. Singh R, Switala J, Loewen PC, Ivancich A (2007) J Am Chem Soc 129:15954–15963
10. Chouchane S, Lippai I, Magliozzo RS (2000) Biochemistry 39:9975–9983
11. Jakopitsch C, Auer M, Regelsberger G, Jantschko W, Furtmuller PG, Ruker F, Obinger C (2003) Biochemistry 42:5292–5300
12. Jakopitsch C, Ivancich A, Schmuckenschlager F, Wanasinghe A, Potl G, Furtmuller PG, Ruker F, Obinger C (2004) J Biol Chem 279:46082–46095
13. Jakopitsch C, Auer M, Regelsberger G, Jantschko W, Furtmuller PG, Ruker F, Obinger C (2003) Eur J Biochem 270:1006–1013
14. Jakopitsch C, Auer M, Ivancich A, Ruker F, Furtmuller PG, Obinger C (2003) J Biol Chem 278:20185–20191
15. Regelsberger G, Jakopitsch D, Ruker F, Krois D, Peschek GA, Obinger C (2000) J Biol Chem 275:22854–22861
16. Jakopitsch C, Vlasits J, Wiseman B, Loewen PC, Obinger C (2007) Biochemistry 46:1183–1193
17. Ghiladi RA, Knudsen GM, Medzihradszky KF, Ortiz de Montellano PR (2005) J Biol Chem 280:22651–22663
18. Spotilak T, Dawson JH, Ballou DP (2005) J Biol Chem 280:20300–20309
19. Carpena X, Switala J, Loprasert S, Mongkolsuk S, Fita I, Loewen PC (2002) Acta Crystallogr D 58:2184–2186
20. Rørth M, Jensen PK (1967) Biochim Biophys Acta 139:171–173
21. Childs RE, Bardsley WG (1975) Biochem J 145:93–103
22. Layne E (1957) Methods Enzymol 3:447–454
23. Carpena X, Wiseman B, Deemagarn T, Herguedas B, Ivancich A, Singh R, Loewen PC, Fita I (2006) Biochemistry 45:5171–5179

24. Emsley P, Cowtan K (2004) Acta Crystallogr D 60:2126–2132
25. Deemagarn T, Wiseman B, Carpena X, Ivancich A, Fita I, Loewen PC (2007) Proteins 66:219–228
26. Schonbaum GR (1973) J Biol Chem 248:502–511
27. Henriksen A, Schuller DJ, Meno K, Welinder KG, Smith AT, Gajhede M (1998) Biochemisty 37:8054–8060
28. Loewen PC, Carpena X, Rovira C, Haas R, Odenbreit S, Nicholls P, Fita I (2004) Biochemistry 43:3089–3103
29. Dunford HB (1999) Heme peroxidases. Wiley, New York
30. Fielding AJ, Singh R, Boscolo B, Loewen PC, Ghibaudi EI, Ivancich A (2008) Biochemistry 47:9781–9792
31. Ivancich A, Jakopitsch C, Auer M, Un S, Obinger C (2003) J Am Chem Soc 125:14093–14102
32. Erman JE, Vitello LB, Mauro JM, Kraut J (1989) Biochemistry 28:7992–7995
33. Rodriguez-Lopez JN, Smith AT, Thorneley RNF (1996) J Biol Chem 271:4023–4030
34. Loew G, Dupuis M (1996) J Am Chem Soc 118:10584–10587
35. Derat E, Shaik S, Rovira C, Vidossich P, Alfonso-Prieto M (2007) J Am Chem Soc 129:6346–6347